Published in final edited form as:
J Immunol. 2008 November 1; 181(9): 6236–6243.

n-3 polyunsaturated fatty acids suppress the localization and activation of signaling proteins at the immunological synapse in murine CD4+ T cells by affecting lipid raft formation[1]

Wooki Kim[*], **Yang-Yi Fan**[*], **Rola Barhoumi**[†,‡], **Roger Smith**[§], **David N. McMurray**[*,†,‡,¶], and **Robert S. Chapkin**[*,†,‡,2]

[*]*Faculty of Nutrition, Texas A&M University, College Station, TX 77843*

[†]*Center for Environmental and Rural Health, Texas A&M University, College Station, TX 77843*

[‡]*Department of Veterinary Integrative Biosciences, Texas A&M University, College Station, TX 77843*

[§]*Department of Veterinary Pathology, Texas A&M University, College Station, TX 77843*

[¶]*Department of Microbial & Molecular Pathogenesis, Texas A&M University System Health Science Center, College Station, TX 77843*

Abstract

The molecular properties of immunosuppressive n-3 polyunsaturated fatty acids (PUFA) have not been fully elucidated. Using $CD4^+$ T cells from wild type control and *fat-1* transgenic mice (enriched in n-3 PUFA), we show that membrane raft accumulation assessed by Laurdan (6-dodecanoyl-2-dimethyl aminonaphthalene) labeling was enhanced in *fat-1* cells following immunological synapse (IS) formation by CD3-specific Ab expressing hybridoma cells. However, the localization of PKCθ, PLCγ-1 and F-actin into the IS was suppressed. In addition, both the phosphorylation status of PLCγ-1 at the IS and cell proliferation as assessed by CFSE labeling and [^{3}H]-thymidine incorporation were suppressed in *fat-1* cells. These data imply that lipid rafts may be targets for the development of dietary agents for the treatment of autoimmune and chronic inflammatory diseases.

Keywords

T cells; Signal Transduction; Cell Activation; fat-1; immunological synapse; lipid rafts; nutrition

Introduction

The Singer and Nicholson lipid bilayer model of the plasma membrane (1) has evolved significantly to include specialized microdomains, i.e., lipid rafts. Lipid rafts can be classified as morphologically featureless, detergent-resistant membranes (DRM)[3] due to their

[1]This work was supported by National Institutes of Health Grants DK071707, CA59034 and P30ES09106. Confocal and multi-photon microscopy was performed in the College of Veterinary Medicine & Biochemical Sciences Image Analysis Laboratory, supported with funding from NIH-NCRR Shared Instrumentation Grant (1 S10 RR22532-01)

[2]Address correspondence and reprint request to Dr. Robert S. Chapkin, 321 Kleberg Biotechnology Center, MS 2253, Texas A&M University, College Station, TX 77843-2253, USA. Phone: 979-845-0448, Fax: 979-862-2378, E-mail: r-chapkin@tamu.edu

[3]Abbreviations used in this paper: DRM, detergent-resistant membranes; PUFA, polyunsaturated fatty acids; DHA, docosahexaenoic acid; PKC, protein kinase C; CARMA1, caspase recruitment domain-containing protein 11; EPA, eicosapentaenoic acid; MβCD, methyl-β-cyclodextrin; GP, generalized polarization; LAT, linker for activation of T cells; PLC, phospholipase C; CTx-FITC, cholera toxin B subunit-fluorescein isothiocyanate; RRI, relative relocation index; PI, propidium iodide; DPM, disintegrations per minute

insolubility in cold nonionic detergents (2). Their highly enriched cholesterol and sphingolipid content suggests that they are in a liquid ordered (l_o) state, whereas the bulk membrane is in a liquid disordered (l_d) state (3). The biochemical characterization of lipid rafts has provided new insight into the regulation and function of plasma membrane proteins. For example, it is now known that T cell intracellular signaling cascades, endocytosis, protein trafficking and cell-cell communication are modulated in part by altering the lipid-protein composition of the bulk membrane and specialized lipid microdomains (3-6).

Dietary fish oil, rich in n-3 polyunsaturated fatty acids (PUFA), can alter immune cell function and aid in the resolution of chronic inflammation, e.g., arthritis, Crohn's disease, dermatitis, psoriasis and ulcerative colitis (7-10). To further investigate the anti-inflammatory properties of fish oil, we have demonstrated that n-3 PUFA modulate $CD4^+$ T cell immune responses in part via reduction in Th1 clonal expansion (11), IL-2 secretion and IL-2 receptor α-chain mRNA transcription (12). However, the molecular mechanisms by which n-3 PUFA suppress $CD4^+$ T cell function are not fully understood.

It has been reported that the fatty acid composition of lipid rafts and the bulk membrane in Jurkat T cells was altered by addition of n-3 PUFA to the culture media (13). Our lab also demonstrated the modulation of T cell lipid rafts by dietary n-3 PUFA in a mouse model (14). In the latter study, it was demonstrated that dietary fish oil as well as purified docosahexaenoic acid (DHA, 22:6n-3), a major bioactive n-3 PUFA, altered $CD4^+$ T cell plasma membrane fatty acid composition, specifically in phosphatidylserine and phosphatidylethanolamine, which are abundant in the cytofacial leaflet of the cell membrane (15). In contrast, fatty acid profiles in sphingomyelin, phosphatidylinositol, and phosphatidylcholine, which are major lipids in the exofacial leaflet (15) in which TCR is linked, were not altered. These observations may partially explain why n-3 PUFA alter signaling pathways without affecting expression and/or affinity of the TCR/CD3 complex (16,17). Furthermore, in complementary studies, changes in lipid raft fatty acid composition were associated with a decrease in the translocation of protein kinase C (PKC)θ, a key molecule regulating $CD4^+$ T cell activation, into lipid rafts in mitogen stimulated T cells (12). In contrast, n-3 PUFA incubation displaced F-actin, talin, LFA-1α, but not PKCθ from the IS, where T cells and APC form a conjunction (18). In terms of cell signaling triggered by TCR, it was reported that a scaffold protein, caspase recruitment domain-containing protein 11 (CARD11, CARMA1) is recruited into the IS and plays an essential role in linking Ag recognition, PKCθ activation via translocation into lipid rafts and NF-kB nuclear translocation (19). From these studies, it is apparent that n-3 PUFA may modulate T cell function via alteration of lipid raft structure and the translocation of signaling molecules.

We have recently reported that long chain PUFA alter the size and distribution of lipid rafts in HeLa cells, as determined by immuno-gold electron microscopy (20). These data suggest that plasma membrane organization of inner leaflets is fundamentally altered by n-3 PUFA enrichment. However, to date, the direct visualization of T cell lipid rafts at the IS following n-3 PUFA membrane enrichment has not been reported. Recently, it was demonstrated that the fluorescent probe Laurdan can align itself parallel with the hydrophobic tails of phospholipids in membranes (21-23). Owing to its ability to emit two different wavelengths according to the fluidity of the microenvironment, Laurdan can be used to measure membrane fluidity and visualize lipid rafts in living cells by two-photon microscopy (22).

Since mammals cannot produce n-3 PUFA from the major n-6 PUFA found in the diet due to the lack of Δ15-desaturase activity, it is necessary to enrich the diet with eicosapentaenoic acid (EPA, 20:5n-3) and/or DHA in order to assess their biological properties *in vivo*. Recently, the *fat-1* gene encoding an n-3 fatty acid desaturase was cloned from *Caenorhabditis elegans* and expressed in mammalian cells (24). This enzyme can catalyze the conversion of n-6 PUFA to

n-3 PUFA by introducing a double bond into fatty acyl chains. Hence, transgenic mice expressing *fat-1* allow us to investigate the biological properties of n-3 PUFA without having to incorporate these fatty acids in the diet. Using the *fat-1* mouse model, we report for the first time the effect of n-3 PUFA on (a) the formation of lipid rafts in living $CD4^+$ T cells at the immunological synapse, (b) membrane translocation of signaling molecules, (c) phosphorylation (activation status) of key signaling proteins and (d) the proliferation of $CD4^+$ T cells.

Materials and Methods

Animals, diets, and $CD4^+$ T cell purification

Fat-1 transgenic mice were generated and backcrossed onto a C57BL/6 background by breeding heterozygous mice (24,25). Littermates were used in all experiments as previously described (25). All procedures followed guidelines approved by Public Health Service and the Institutional Animal Care and Use Committee at Texas A&M University. Mice were genotyped using tail DNA. To confirm the phenotype, total lipids were isolated from splenic $CD4^+$ T cells and the fatty acid profile was characterized by gas chromatography as previously described (14). Animals were fed a 10% safflower oil diet (n-6 PUFA rich, Research Diets) *ad libitum* with a 12 h light/ dark cycle. The diet contained 40 (g/100 g diet) sucrose, 20 casein, 15 corn starch, 0.3 DL-methionine, 3.5 AIN 76A salt mix, 1.0 AIN 76A mineral mix, 0.2 choline chloride, 5 fiber (cellulose), 10 safflower oil. $CD4^+$ T cells from *fat-1* or WT mice were isolated from spleens by a magnetic microbead positive selection method (Miltenyi Biotec) according to the manufacturer's recommendation.

Laurdan labeling

Purified (91.0 ± 1.0% determined by flow cytometry, n=3) $CD4^+$ T cells were stained with Laurdan (Invitrogen) for lipid raft visualization. Briefly, 5 μmol/L Laurdan was prepared in serum-free RPMI medium and incubated with 2×10^6 cells/mL for 30 min at 37°C (21). Cells were subsequently washed and resuspended in serum-free Leibovitz's medium. To evaluate the effect of cholesterol depletion on lipid raft formation, cells were pretreated with 10 mmol/L methyl-β-cyclodextrin (MβCD, Sigma) in fatty acid-free RPMI media containing 0.1% BSA for 3 min prior to Laurdan labeling (26).

$CD4^+$ T cell activation and two-photon microscopy

For mitogenic activation, $CD4^+$ T cells were cocultured with CD3-specifc Ab expressing hybridoma cells (clone 145-2C11, ATCC, anti-CD3 hybridoma) in complete medium [RPMI 1640 medium with 25 mmol/L HEPES (Irvine Scientific), supplemented with 5% heat-inactivated FBS (Invitrogen), 10^5 U/L penicillin and 100 mg/L streptomycin (Gibco), 2 mmol/L L-glutamine (Glutamax®, Gibco), and 10 μmol/L 2-ME (Sigma)]. To validate immune synapse formation, T cells were also incubated with an irrelevant DNP-specific Ab expressing hybridoma cells (clone UC8-1B9, anti-DNP hybridoma) (27). In select experiments, hybridoma cells were prelabeled with Cell Tracker orange-fluorescent tetramethylrhodamine (CMTMR, Invitrogen). Laurdan labeled $CD4^+$ T cells were coincubated with hybridoma cells at a ratio of 5:1. Cell mixtures were seeded onto poly-L-lysine (Sigma) precoated chambered coverglass slides (2×10^6 $CD4^+$ T cells/chamber). After a 30 min incubation period at 37°C, Laurdan was measured by two-photon microscopy (Zeiss LSM 510 META NLO, 40x objective 1.3 NA oil) at 400-460 nm and 470-530 nm (Fig. 1A-D) to calculate generalized polarization (GP)-values, which indicate l_o and l_d states of the membrane, respectively (22). The Coherent Chameleon femtosecond pulsed Ti:Sapphire laser was set at an excitation of 770 nm.

GP-value calculation

All images were converted to 8-bit/channel TIFF format and were processed using Adobe Photoshop CS3®. The mean intensities of each color channel were measured in either whole cells or contact regions of the synapse by drawing a polygon around each cell boundary (whole cell) (Fig. 1F) or by drawing an oval at the T cell membrane proximal to the hybridoma cell (Fig. 1E). GP-values were obtained by the formula, $GP=(I_{400-460}-I_{470-530})\div(I_{400-460}+I_{470-530})$, where I stands for intensities of each region of interest for the blue and green channels, respectively (21,22).

Quantification of protein localization, activation and GM1 relocation

To assess the relocalization of signaling proteins or cytoskeletal F-actin, isolated $CD4^+$ T cells were mixed with hybridoma cells (5:1) and seeded onto poly-L-lysine precoated coverglass slides. After a 30 min incubation period, cells were fixed in 4% formaldehyde for 20 min, rinsed with PBS, and incubated with 10 mmol/L glycine in PBS for 10 min at room temperature to quench aldehyde groups. Cell membranes were permeabilized by exposure to 0.2% Triton X-100 in PBS for 5 min at room temperature, followed by PBS washing. Cells were subsequently covered with blocking solution (1% BSA/0.1% NaN_3 in PBS) and incubated at 4°C overnight with primary Abs, rabbit Abs specific to either PKCθ (Santa Cruz Biotechnology), linker for activation of T cells (LAT), phospho-LAT (Upstate Biotechnology), CARMA1, phospholipase C (PLC)γ-1, phospho-PLCγ-1 (Cell Signaling Technology) as previously reported (12). After PBS washing, cells were incubated with secondary Alexa Fluor® 568 goat Ab to rabbit IgG (Molecular Probes). In order to visualize F-actin and ganglioside GM1 localization, cells were incubated with F-actin-specific phallotoxin-Alexa Fluor 568® (Molecular Probes) or GM1-specific cholera toxin B subunit-fluorescein isothiocyanate (CTx-FITC, Sigma), respectively. Following serial ethanol dehydration steps, samples were mounted onto glass slides with ProLong Antifade reagent (Molecular Probes) (12). Fluorescence images were acquired by confocal microscopy to determine both the translocation and phosphorylation status (activation) of signaling proteins in $CD4^+$ T cells. Either a BioRad Radiance 2000MP (argon laser excitation at 568 nm and emission at 590 nm, 63x objective 1.4 NA water) or Zeiss LSM 510 META NLO (argon laser excitation at 543 nm and emission with a LP 560 nm, 63x objective 1.4 NA oil) system was used for image acquisition. Cell images were captured in 8-bit TIFF format and the percentage of cells with protein patching at the IS was counted to assess the relocalization of signaling proteins or F-actin. GM1 recruitment into the IS was quantified by relative relocation index (RRI) (28). Briefly, polygons were drawn to designate the IS, the contact whole cell and background area. RRI was calculated by the formula, RRI=[mean fluorescence intensity (MFI) at the IS-background]÷(MFI at the contact whole cell-background). Quantitative analysis of MFI was performed using Adobe Photoshop® CS3 for Windows.

$CD4^+$ T cell proliferation assay

The effect of n-3 PUFA on T cell proliferation was evaluated by the [^{3}H]-thymidine incorporation and CFSE labeling as previously described (11,29). Briefly, 2×10^5 purified $CD4^+$ T cells were stimulated using either control RPMI complete medium, 5×10^5 anti-CD3 hybridoma cells which were pretreated with 10 μmol/L mitomycin C (Sigma) for 30 min to block cell division, plate bound CD3-specific mAb (1 ng/L) and soluble CD28-specific mAb (5 ng/L, BD Pharmingen) (anti-CD3/28 mAbs) or PMA (1 pg/L) and Ionomycin (500 nmol/L) (PMA/Ionomycin). Cells were cultured for 72 h in round-bottom 96-well multiplates. For CFSE profile analysis, $CD4^+$ T cells were pretreated with 5 μmol/L CFSE in PBS supplemented with 5% FBS for 10 min (29). After 72 h in culture as described above, CFSE was analyzed by flow cytometry (FACSCalibur, BD) as previously reported (11). Briefly, cells were harvested by centrifugation and resuspended in PBS. To determine viability, propidium iodide

(PI, Sigma) was added to each sample prior to analysis. CFSE fluorescence was detected using a 530/30 band pass filter and PI fluorescence through a 650LP filter. CFSE fluorescence was sufficiently intense to be detected through a 650LP filter. Viable cells were determined using a plot of CFSE vs PI fluorescence, based on the fluorescence patterns of a sample with CFSE but no PI. This gate also excluded most of the hybridoma cells because of their higher level of autofluorescence. An additional lymphocyte gate was set based on forward and side light scattering properties. CFSE profiles were analyzed by ModFit LT 3.0 (Verity Software House). Data were expressed as difference of percentage (Δpercentage, *fat-1* - WT) at each daughter cell generation. For the [^{3}H]-thymidine incorporation, 4 μCi [^{3}H]-thymidine/well (New England Nuclear) was added to the cultures for the final 6 h. Cells were harvested using a 96-well cell harvester (Packard Instrument) and thymidine uptake was measured using liquid scintillation counting (Beckman Coulter). Results are expressed as proliferation index, which is derived by dividing disintegrations per minute (DPM) of stimulated wells by DPM of basal control.

Statistics

Data were analyzed using Student's t-test to compare *fat-1* and WT cells. Kolmogorov-Smirnov method was applied to test the normality of the data distribution. Statistical interaction of the variables (genotype and ROI) was tested by two-way ANOVA. To compare multiple treatment means, one-way ANOVA and LSD multiple post-hoc tests were used (SPSS 15.0 for Windows). Data are expressed as mean ± SEM and differences of $P<0.05$ were considered statistically significant.

Results

n-3 PUFA enhances the formation of lipid rafts at the immune synapse

Both *fat-1* transgenic and wild type (WT) control offspring were fed a 10% safflower oil diet enriched in n-6 PUFA throughout the duration of study. Splenic CD4$^+$ T cell total lipid fatty acid compositional analyses revealed an increase in n-3 PUFA [EPA (P=0.010), docosapentaenoic acid (DPA 22:5n-3, P=0.007) and DHA (P=0.015)] and a decrease in n-6 PUFA, specifically arachidonic acid (20:4n-6, P=0.053), adrenic acid (22:4n-6, P=0.041) and DPA (22:5n-6, P=0.008) in *fat-1* transgenic mice (Fig.2). In addition, the ratio of n-6 to n-3 PUFA was significantly (P=0.003) suppressed in *fat-1* (5.13 ± 1.18), compared to WT T cells (35.71 ± 6.38). These data indicate that an appropriate activity of n-3 fatty acid desaturase was present and that T cells from *fat-1* mice were enriched in n-3 PUFA.

To investigate the effect of endogenous n-3 PUFA on lipid raft formation at the IS, Laurdan labeled CD4$^+$ T cells were cocultured with anti-CD3 hybridoma cells at 37°C in 5% CO_2 for 30 min. Images of conjugate CD4$^+$ T cells and hybridomas were captured, while non-contact CD4$^+$ T cells served as a negative control. Two-way ANOVA of generalized polarization (GP)-values revealed that there was no statistical interaction between genotype and regions of interest (ROI) (P=0.430). GP-values were significantly ($P<0.001$, LSD post-hoc test) increased at the IS (0.412 ± 0.017 WT vs 0.452 ± 0.014 *fat-1*) compared to non-contact T cells (0.329 ± 0.008 WT vs 0.372 ± 0.008 *fat-1*) or contact whole cells (0.363 ± 0.010 WT vs 0.377 ± 0.008 *fat-1)* (Fig. 3A). Overall, raft formation was enhanced in *fat-1* vs WT cells in both resting (P=0.016) and stimulated (P=0.022) CD4$^+$ T cells. The DNP-specific Ab expressing hybridoma was used as a negative control, and failed to exhibit an increase in the GP index at the IS (Fig. 3B and C). These data demonstrate that the n-3 PUFA-dependent increase in the GP index is IS dependent.

In independent experiments, CD4$^+$ T cells were pretreated with 10 mmol/L MβCD for 3 min to specifically deplete cholesterol from lipid rafts as described previously (26). Laurdan

analysis revealed that the elevated GP values associated with IS formation (ΔGP=0.195 ± 0.030, *fat-1* and 0.139 ± 0.015, WT, n=6-14 cells per mouse from 1-2 mice per genotype) was diminished following MβCD treatment (ΔGP=0.053 ± 0.022, *fat-1* and ΔGP=0.059 ± 0.033, WT), indicating that changes in the GP index at the IS are cholesterol dependent.

In complementary experiments, GM1-specific microcluster recruitment was assessed using CTx-FITC. CTx has been used to mark membrane microdomains in the exofacial leaflet, although a significant fraction of GM1 is found outside l_o regions (30). Interestingly, in contrast to the enhanced l_o domain formation at the IS (Fig. 3B), GM1 recruitment was not altered in *fat-1* $CD4^+$ T cells (Fig. 3D and E).

n-3 PUFA suppress the localization of signaling proteins into the IS

Following Ag recognition by the TCR, signaling cascades proximal to the IS are initiated by relocalization of a complex of molecules, i.e., protein kinases (Fyn, Lck, ZAP-70, PLCγ-1), scaffolding proteins (LAT, Grb-2, SLP-76, CARMA1) and cytoskeletal proteins (F-actin) into the IS (5,19,31). In this study, the effect of n-3 PUFA on the localization of select signaling molecules in the plasma membrane at the IS was quantified. Fig. 4A shows representative cell images obtained following incubation with rabbit mAb specific to mouse LAT and the secondary Alexa Fluor® 568 Ab specific to rabbit IgG. Relocalization of PKCθ, PLCγ-1 and F-actin into the IS, expressed as the percentage conjugate with patching, were suppressed in *fat-1* transgenic cells by 30% (P=0.050), 32% (P=0.081) and 36% (P=0.020), respectively (Fig. 4B). In contrast, the intracellular localization of LAT and CARMA1 at the IS was not altered by n-3 PUFA.

n-3 PUFA down-regulate PLCγ-1 phosphorylation at the IS

Since phosphorylation of LAT and PLCγ-1 occurs at the very early stages of T cell activation, either phospho-LAT or phospho-PLCγ-1 specific Ab was used to visualize the effect of n-3 PUFA on T cell activation. Specifically, the percentage conjugate patching of phospho-Y195 (LAT) (32) and phospho-Y783 (PLCγ-1) (33) was examined and showed that PLCγ-1 phosphorylation was suppressed by 29% (P=0.034) in n-3 PUFA enriched cells at the IS, whereas LAT phosphorylation was not altered (P=0.464) (Fig. 5A and B).

n-3 PUFA suppress $CD4^+$ T cell proliferation

$CD4^+$ T cells were labeled with CFSE and cultured for 72 h for the purpose of determining whether the effect of n-3 PUFA on lipid rafts and signaling protein recruitment/activation was associated with an alteration in T cell proliferation. Using flow cytometry analysis, non-viable cells were gated out based on their uptake of PI (Fig. 6A, D and G) and lymphocytes were identified by forward and side scatter plot analysis (Fig. 6B, E and H). The parental peak was obtained by examining unstimulated control cells, which did not divide (Fig. 6C), whereas cell division was visualized by the shift of CFSE peak to the left (11, 29). To identify each daughter generation, computer-aided modeling was performed (Fig. 6F and I). Examination of the percentage of each daughter cell generation revealed that *fat-1* $CD4^+$ T cell proliferation was suppressed in response to anti-CD3 hybridoma stimulation. Specifically, a higher percentage of non-divided parental cells (Δpercentage=5.87, P=0.028) and lower percentage of daughter cells at generation 4 (Δpercentage=−0.98, P=0.037), 5 (Δpercentage=−1.73, P=0.042) and 6 (Δpercentage=−1.38, P=0.065) were obtained (Fig. 7A). In addition, $CD4^+$ T cells stimulated by either anti-CD3/28 mAbs or PMA/Ionomycin exhibited a similar trend; larger fraction at generation 1 (Δpercentage=4.30, P=0.085 anti-CD3/28 mAbs, Δpercentage=3.58, P=0.001 PMA/Ionomycin) and a reduced number of cells at generation 4 (Δpercentage=−3.34, P=0.081 anti-CD3/28 mAbs), suggesting a suppression of cell division in the *fat-1* group (Fig. 7B and C).

In a complementary experiment, $CD4^+$ T cell proliferation was assessed by the incorporation of [^{3}H]-thymidine. In accordance with CFSE profile data, thymidine uptake expressed as the proliferation index revealed that *fat-1* $CD4^+$ T cell division was significantly suppressed by 52% ($P<0.001$), 45% ($P=0.002$) and 56% ($P=0.001$) in anti-CD3 hybridoma, anti-CD3/28 mAbs and PMA/Ionomycin stimulated cells, respectively (Fig. 8).

Discussion

It has been postulated that n-3 PUFA, because of their perceived broad acting effects on mammalian physiology, act at a fundamental level common to all cells, i.e., by altering the physical properties of biological membranes (9,10,18,34-38). More specifically, we hypothesized that the anti-inflammatory effects of n-3 PUFA on $CD4^+$ T cells would be explained, in part, by suppressing/disrupting lipid raft formation at the IS.

To elucidate the membrane bioactive properties of n-3 PUFA in T-cells, the *fat-1* transgenic mouse model was utilized because it is uniquely capable of converting n-6 PUFA to n-3 PUFA endogenously by introducing a cis double bond into fatty acyl chains (24,39). Data from initial experiments showed that the *fat-1* gene was functionally expressed in splenic $CD4^+$ T cells and that the plasma membrane was enriched in n-3 PUFA (Fig. 2).

We have demonstrated previously that n-3 PUFA suppress murine $CD4^+$ T cell proliferation by remodeling lipid raft fatty acid composition and by altering PKCθ colocalization (12). In that study, $CD4^+$ T cells were stimulated by culture plate-bound mAb to CD3 (anti-CD3 mAb) to induce the colocalization of PKCθ with GM1, a marker of lipid rafts. However, the direct visualization of lipid rafts at the IS is necessary in order to investigate microdomain assembly and localization at the plasma membrane. Hence, in the present study, we incubated $CD4^+$ T cells with Laurdan to directly measure membrane fluidity and visualize lipid rafts by two-photon microscopy. For this purpose, anti-CD3 hybridoma cells were used as Ag presenting cells to form an IS, since they express cell surface costimulatory B7 and intercellular adhesion molecule (ICAM-1) (27). In a major step toward developing a unifying mechanistic hypothesis addressing how dietary PUFA modulate cell membrane microdomains, we demonstrate for the first time that n-3 PUFA actually promote lipid raft formation at the IS (Fig. 3A-C). These results can be explained in part by the fact that n-3 PUFA, specifically DHA, has a low affinity for cholesterol, providing a lipid-driven mechanism for lateral phase separation of cholesterol/sphingolipid-rich lipid microdomains from the surrounding l_d phase (34-38). Hence, the insertion of DHA into the bulk membrane should enhance the coalescence of cholesterol-rich lipid raft-like domains in living cells. These findings are consistent with previous observations using immuno-gold electron microscopy of plasma membrane sheets coupled with spatial point analysis of validated microdomain markers (20). In that study, we demonstrated that DHA increased lipid raft clustering in HeLa cells, indicating that plasma membrane organization of inner leaflets is fundamentally altered by n-3 PUFA-enrichment.

With regard to the role of lipid rafts in T cell activation, T cells from patients suffering from autoimmune disease synthesized more GM1 following TCR activation (5), suggesting that GM1 enriched domains play a critical role in the activation of immune responses. However, cholesterol overloading in healthy T cells reduced the lateral mobility of receptors and signaling molecules providing a link between plasma membrane cholesterol content and immunosenescence (5). These observations are controversial because GM1 and cholesterol, which are both thought to be lipid raft building blocks (3), play different roles in T cell activation and regulation. Therefore, we measured the recruitment of GM1 into the IS by labeling with CTx-FITC in order to evaluate the effect of n-3 PUFA on GM1-specific lipid rafts. Of interest, GM1 relocation as assessed by RRI was not altered by n-3 PUFA (Fig. 3E). This observation is consistent with a previous report, where GM1 localization as assessed by

biochemical isolation of DRM was not affected by PUFA treatment (40). Interestingly, the fatty acid composition of phospholipids in the exofacial leaflet of T cells, where GM1 is enriched, was not altered by n-3 PUFA (14). In addition, long chain PUFA are predominantly enriched in phospholipids localized to the cytofacial leaflet (14,41). Based on these findings, the data suggest that the incorporation of n-3 PUFA into cytofacial leaflet phospholipids alters the lateral composition of lipid rafts in the plasma membrane, thereby altering the IS microenvironment to impact thresholds for the activation TCR mediated cell signaling.

The proximal events of cell signaling following Ag recognition by the TCR are initiated by the localization of signaling molecules into the IS (5). To evaluate the effect of n-3 PUFA on the localization of select signaling proteins, the percentage of cells with multi-protein signaling complexes relocalized to the IS was enumerated by immunofluorescence microscopy. Consistent with a perturbation in lipid raft structure, n-3 PUFA enriched $CD4^+$ T cells exhibited a suppressed localization of PKCθ, PLCγ-1 and F-actin into the IS (Fig. 4). We also reported that PKCθ colocalization with GM1 in anti-CD3 mAb stimulated T cells was suppressed by dietary fish oil and purified DHA ethyl ester administration (12). Although a significant fraction of GM1 can be found outside l_o regions (30,42), the dislocation of PKCθ from GM1 enriched domains may explain in part why PKCθ accumulation at the IS was suppressed by n-3 PUFA, while lipid raft formation was enhanced. In addition, we also show that the localization of PLCγ-1 and F-actin was selectively suppressed by n-3 PUFA, whereas LAT and CARMA1 localization was not altered. In contrast, in a previous study, F-actin, LAT and PKCθ localization into the IS was not altered by n-3 PUFA (EPA) treatment compared to n-6 PUFA (arachidonic acid) (18). Indeed, both n-3 and n-6 PUFA treatment equally suppressed the localization of F-actin, talin, leukocyte function-associated molecule-1α, LAT and CD3ε into the IS, compared to the saturated stearic acid (18:0) treated control group. The apparent differences between these studies may be attributed to the fact that Jurkat human T cells were directly incubated with 50 μmol/L fatty acid followed by antigenic stimulation (18).

Since not only the spatial migration but also the phosphorylation status of LAT and PLCγ-1 is critical for T cell activation (32,33) and dietary FO has been shown to modulate PLCγ-1 phosphorylation in rat lymphocytes (43), we counted cells with phospho-specific immunofluorescent patching in order to assess the activation status of those proteins. In accordance with the localization results, LAT phosphorylation was not affected by n-3 PUFA, however PLCγ-1 phosphorylation was suppressed in *fat-1* transgenic T cells (Fig. 5). These data indicate that n-3 PUFA selectively modulate the localization and/or activation status of signaling proteins in TCR-mediated T cell activation.

The function of the IS is still evolving. For example, membrane condensation and signaling protein translocation to the IS has been shown to be critical for TCR triggered T cell activation (21). In contrast, compelling data suggest central supramolecular activation cluster (cSMAC) of mature IS may promote TCR/CD3 internalization and recycling (44). In addition, TCR microclusters initiate T cell signaling in seconds (45) following binding to peptide-MHC complex but the signal becomes weaker when cSMAC is formed in minutes (46,47). These observations suggest that the dynamic nature of the IS and perhaps rapid formation/dissolution of rafts promote TCR signaling. It is possible, therefore, that n-3 PUFA by stabilizing lipid rafts at the IS disrupt lipid-protein interactions and perturb membrane structure/function.

Alteration of $CD4^+$ T cell lipid raft microdomains and proximal T cell signaling by n-3 PUFA in *fat-1* cells resulted in the suppression of proliferation (Fig. 7A and 8), indicating the critical importance of lipid raft localization of proteins such as PKCθ, PLCγ-1 and F-actin to TCR signaling. To test if the mechanism of suppression by n-3 PUFA was limited to the IS or proximal signaling cascades, T cells were stimulated with either anti-CD3/28 mAbs or PMA/Ionomycin to bypass IS formation and TCR mediated signaling, respectively. T cell

proliferation by anti-CD3/28 mAbs and PMA/Ionomycin was suppressed as assessed by CFSE profiles and thymidine uptake, indicating that the down-regulation of T cell proliferation by n-3 PUFA is not limited to TCR-mediated activation. Indeed, CFSE profile analysis revealed that the largest Δpercentage was associated with the non-dividing parental generation when T cells were stimulated with the IS forming anti-CD3 hybridoma cell model (Fig. 7), consistent with a very strong suppression of T cell proliferation. These data are consistent with previous reports that n-3 PUFA are anti-inflammatory and immunomodulatory in vivo (12,48).

In general, hyperactivation of $CD4^+$ T cells is associated with enhanced susceptibility to autoimmune disorders and chronic inflammatory diseases induced diseases (9,10). Recently, our lab reported that *fat-1* mice exhibited an enhanced ability to resolve dextran sodium sulphate-induced intestinal inflammation and injury (25). Since subsets of $CD4^+$ T cells are known to be critical mediators of chronic inflammation, results from our study may partially explain why n-3 PUFA favorably modulate the inflammation-dysplasia-carcinoma axis.

In conclusion, we have shown that n-3 PUFA promote the formation of lipid rafts and perturb the reorganization of signaling machinery which is critical to T cell activation. These results provide a critical new paradigm in understanding the molecular mechanisms through which dietary n-3 PUFA modulate T-cell activation. Additional studies are needed to further elucidate the effect of dietary n-3 PUFA on T cell signaling networks.

Acknowledgement

We thank J. X. Kang, Department of Medicine, Harvard University, for providing *fat-1* breeder mice and L. Zhou for statistical assistance.

References

1. Singer SJ, Nicolson GL. The fluid mosaic model of the structure of cell membranes. Science 1972;175:720–731. [PubMed: 4333397]
2. Lingwood D, Simons K. Detergent resistance as a tool in membrane research. Nat Protoc 2007;2:2159–2165. [PubMed: 17853872]
3. Pike LJ. Lipid rafts: heterogeneity on the high seas. Biochem J 2004;378:281–292. [PubMed: 14662007]
4. Hanzal-Bayer MF, Hancock JF. Lipid rafts and membrane traffic. FEBS Lett 2007;581:2098–2104. [PubMed: 17382322]
5. Jury EC, Flores-Borja F, Kabouridis PS. Lipid rafts in T cell signalling and disease. Semin Cell Dev Biol 2007;18:608–615. [PubMed: 17890113]
6. Brassard P, Larbi A, Grenier A, Frisch F, Fortin C, Carpentier AC, Fulop T. Modulation of T-cell signalling by non-esterified fatty acids. Prostaglandins Leukot Essent Fatty Acids 2007;77:337–343. [PubMed: 18042367]
7. Sijben JW, Calder PC. Differential immunomodulation with long-chain n-3 PUFA in health and chronic disease. Proc Nutr Soc 2007;66:237–259. [PubMed: 17466105]
8. Siddiqui RA, Harvey KA, Zaloga GP, Stillwell W. Modulation of lipid rafts by Omega-3 fatty acids in inflammation and cancer: implications for use of lipids during nutrition support. Nutr Clin Pract 2007;22:74–88. [PubMed: 17242459]
9. Chapkin RS, Davidson LA, Ly L, Weeks BR, Lupton JR, McMurray DN. Immunomodulatory effects of (n-3) fatty acids: putative link to inflammation and colon cancer. J Nutr 2007;137:200S–204S. [PubMed: 17182826]
10. Chapkin RS, McMurray DN, Lupton JR. Colon cancer, fatty acids and anti-inflammatory compounds. Curr Opin Gastroenterol 2007;23:48–54. [PubMed: 17133085]
11. Zhang P, Kim W, Zhou L, Wang N, Ly LH, McMurray DN, Chapkin RS. Dietary fish oil inhibits antigen-specific murine Th1 cell development by suppression of clonal expansion. J Nutr 2006;136:2391–2398. [PubMed: 16920860]

12. Fan YY, Ly LH, Barhoumi R, McMurray DN, Chapkin RS. Dietary docosahexaenoic acid suppresses T cell protein kinase C theta lipid raft recruitment and IL-2 production. J Immunol 2004;173:6151–6160. [PubMed: 15528352]
13. Li Q, Tan L, Wang C, Li N, Li Y, Xu G, Li J. Polyunsaturated eicosapentaenoic acid changes lipid composition in lipid rafts. Eur J Nutr 2006;45:144–151. [PubMed: 16133744]
14. Fan YY, McMurray DN, Ly LH, Chapkin RS. Dietary (n-3) polyunsaturated fatty acids remodel mouse T-cell lipid rafts. J Nutr 2003;133:1913–1920. [PubMed: 12771339]
15. Zachowski A. Phospholipids in animal eukaryotic membranes: transverse asymmetry and movement. Biochem J 1993;294(Pt 1):1–14. [PubMed: 8363559]
16. Chow SC, Sisfontes L, Jondal M, Bjorkhem I. Modification of membrane phospholipid fatty acyl composition in a leukemic T cell line: effects on receptor mediated intracellular Ca2+ increase. Biochim Biophys Acta 1991;1092:358–366. [PubMed: 1646642]
17. Sasaki T, Kanke Y, Kudoh K, Misawa Y, Shimizu J, Takita T. Effects of dietary docosahexaenoic acid on surface molecules involved in T cell proliferation. Biochim Biophys Acta 1999;1436:519–530. [PubMed: 9989281]
18. Geyeregger R, Zeyda M, Zlabinger GJ, Waldhausl W, Stulnig TM. Polyunsaturated fatty acids interfere with formation of the immunological synapse. J Leukoc Biol 2005;77:680–688. [PubMed: 15703198]
19. Tanner MJ, Hanel W, Gaffen SL, Lin X. CARMA1 coiled-coil domain is involved in the oligomerization and subcellular localization of CARMA1 and is required for T cell receptor-induced NF-kappaB activation. J Biol Chem 2007;282:17141–17147. [PubMed: 17428801]
20. Chapkin RS, Wang N, Fan YY, Lupton JR, Prior IA. Docosahexaenoic acid alters the size and distribution of cell surface microdomains. Biochim Biophys Acta 2008;1778:466–471. [PubMed: 18068112]
21. Gaus K, Chklovskaia E, Jessup W, Harder T. Condensation of the plasma membrane at the site of T lymphocyte activation. J Cell Biol 2005;171:121–131. [PubMed: 16203859]
22. Gaus K, Zech T, Harder T. Visualizing membrane microdomains by Laurdan 2-photon microscopy. Molecular membrane biology 2006;23:41–48. [PubMed: 16611579]
23. Rentero C, Zech T, Quinn CM, Engelhardt K, Williamson D, Grewal T, Jessup W, Harder T, Gaus K. Functional implications of plasma membrane condensation for T cell activation. PLoS ONE 2008;3:e2262. [PubMed: 18509459]
24. Kang JX, Wang J, Wu L, Kang ZB. Transgenic mice: fat-1 mice convert n-6 to n-3 fatty acids. Nature 2004;427:504. [PubMed: 14765186]
25. Jia Q, Lupton JR, Smith R, Weeks BR, Callaway E, Davidson LA, Kim W, Fan YY, Yang P, Newman RA, Kang JX, McMurray DN, Chapkin RS. Reduced Colitis-Associated Colon Cancer in Fat-1 (n-3 Fatty Acid Desaturase) Transgenic Mice. Cancer Res 2008;68:3985–3991. [PubMed: 18483285]
26. Zidovetzki R, Levitan I. Use of cyclodextrins to manipulate plasma membrane cholesterol content: evidence, misconceptions and control strategies. Biochim Biophys Acta 2007;1768:1311–1324. [PubMed: 17493580]
27. Tamir A, Eisenbraun MD, Garcia GG, Miller RA. Age-dependent alterations in the assembly of signal transduction complexes at the site of T cell/APC interaction. J Immunol 2000;165:1243–1251. [PubMed: 10903722]
28. Tavano R, Contento RL, Baranda SJ, Soligo M, Tuosto L, Manes S, Viola A. CD28 interaction with filamin-A controls lipid raft accumulation at the T-cell immunological synapse. Nat Cell Biol 2006;8:1270–1276. [PubMed: 17060905]
29. Quah BJ, Warren HS, Parish CR. Monitoring lymphocyte proliferation in vitro and in vivo with the intracellular fluorescent dye carboxyfluorescein diacetate succinimidyl ester. Nat Protoc 2007;2:2049–2056. [PubMed: 17853860]
30. Owen DM, Neil MA, French PM, Magee AI. Optical techniques for imaging membrane lipid microdomains in living cells. Semin Cell Dev Biol 2007;18:591–598. [PubMed: 17728161]
31. Gaide O, Favier B, Legler DF, Bonnet D, Brissoni B, Valitutti S, Bron C, Tschopp J, Thome M. CARMA1 is a critical lipid raft-associated regulator of TCR-induced NF-kappa B activation. Nat Immunol 2002;3:836–843. [PubMed: 12154360]

32. Reynolds LF, de Bettignies C, Norton T, Beeser A, Chernoff J, Tybulewicz VL. Vav1 transduces T cell receptor signals to the activation of the Ras/ERK pathway via LAT, Sos, and RasGRP1. J Biol Chem 2004;279:18239–18246. [PubMed: 14764585]
33. Moore AL, Roe MW, Melnick RF, Lidofsky SD. Calcium mobilization evoked by hepatocellular swelling is linked to activation of phospholipase Cgamma. J Biol Chem 2002;277:34030–34035. [PubMed: 12167665]
34. Shaikh SR, Edidin M. Polyunsaturated fatty acids, membrane organization, T cells, and antigen presentation. Am J Clin Nutr 2006;84:1277–1289. [PubMed: 17158407]
35. Shaikh SR, Edidin MA. Membranes are not just rafts. Chem Phys Lipids 2006;144:1–3. [PubMed: 16945359]
36. Shaikh SR, Cherezov V, Caffrey M, Stillwell W, Wassall SR. Interaction of cholesterol with a docosahexaenoic acid-containing phosphatidylethanolamine: trigger for microdomain/raft formation? Biochemistry 2003;42:12028–12037. [PubMed: 14556634]
37. Wassall SR, Stillwell W. Docosahexaenoic acid domains: the ultimate non-raft membrane domain. Chem Phys Lipids 2008;153:57–63. [PubMed: 18343224]
38. Soni SP, LoCascio DS, Liu Y, Williams JA, Bittman R, Stillwell W, Wassall SR. Docosahexaenoic acid enhances segregation of lipids between : ^{2}H-NMR study. Biophys J 2008;95:203–214. [PubMed: 18339742]
39. Ma DW, Ngo V, Huot PS, Kang JX. N-3 polyunsaturated fatty acids endogenously synthesized in fat-1 mice are enriched in the mammary gland. Lipids 2006;41:35–39. [PubMed: 16555469]
40. Stulnig TM, Berger M, Sigmund T, Raederstorff D, Stockinger H, Waldhausl W. Polyunsaturated fatty acids inhibit T cell signal transduction by modification of detergent-insoluble membrane domains. J Cell Biol 1998;143:637–644. [PubMed: 9813086]
41. Pike LJ, Han X, Gross RW. Epidermal growth factor receptors are localized to lipid rafts that contain a balance of inner and outer leaflet lipids: a shotgun lipidomics study. J Biol Chem 2005;280:26796–26804. [PubMed: 15917253]
42. Blank N, Schiller M, Krienke S, Wabnitz G, Ho AD, Lorenz HM. Cholera toxin binds to lipid rafts but has a limited specificity for ganglioside GM1. Immunol Cell Biol 2007;85:378–382. [PubMed: 17325693]
43. Sanderson P, Calder PC. Dietary fish oil appears to prevent the activation of phospholipase C-gamma in lymphocytes. Biochim Biophys Acta 1998;1392:300–308. [PubMed: 9630688]
44. Lee KH, Dinner AR, Tu C, Campi G, Raychaudhuri S, Varma R, Sims TN, Burack WR, Wu H, Wang J, Kanagawa O, Markiewicz M, Allen PM, Dustin ML, Chakraborty AK, Shaw AS. The immunological synapse balances T cell receptor signaling and degradation. Science 2003;302:1218–1222. [PubMed: 14512504]
45. Huse M, Klein LO, Girvin AT, Faraj JM, Li QJ, Kuhns MS, Davis MM. Spatial and temporal dynamics of T cell receptor signaling with a photoactivatable agonist. Immunity 2007;27:76–88. [PubMed: 17629516]
46. Mossman KD, Campi G, Groves JT, Dustin ML. Altered TCR signaling from geometrically repatterned immunological synapses. Science 2005;310:1191–1193. [PubMed: 16293763]
47. Varma R, Campi G, Yokosuka T, Saito T, Dustin ML. T cell receptor-proximal signals are sustained in peripheral microclusters and terminated in the central supramolecular activation cluster. Immunity 2006;25:117–127. [PubMed: 16860761]
48. Ly LH, Smith R 3rd, Chapkin RS, McMurray DN. Dietary n-3 polyunsaturated fatty acids suppress splenic CD4(+) T cell function in interleukin (IL)-10(−/−) mice. Clin Exp Immunol 2005;139:202–209. [PubMed: 15654818]

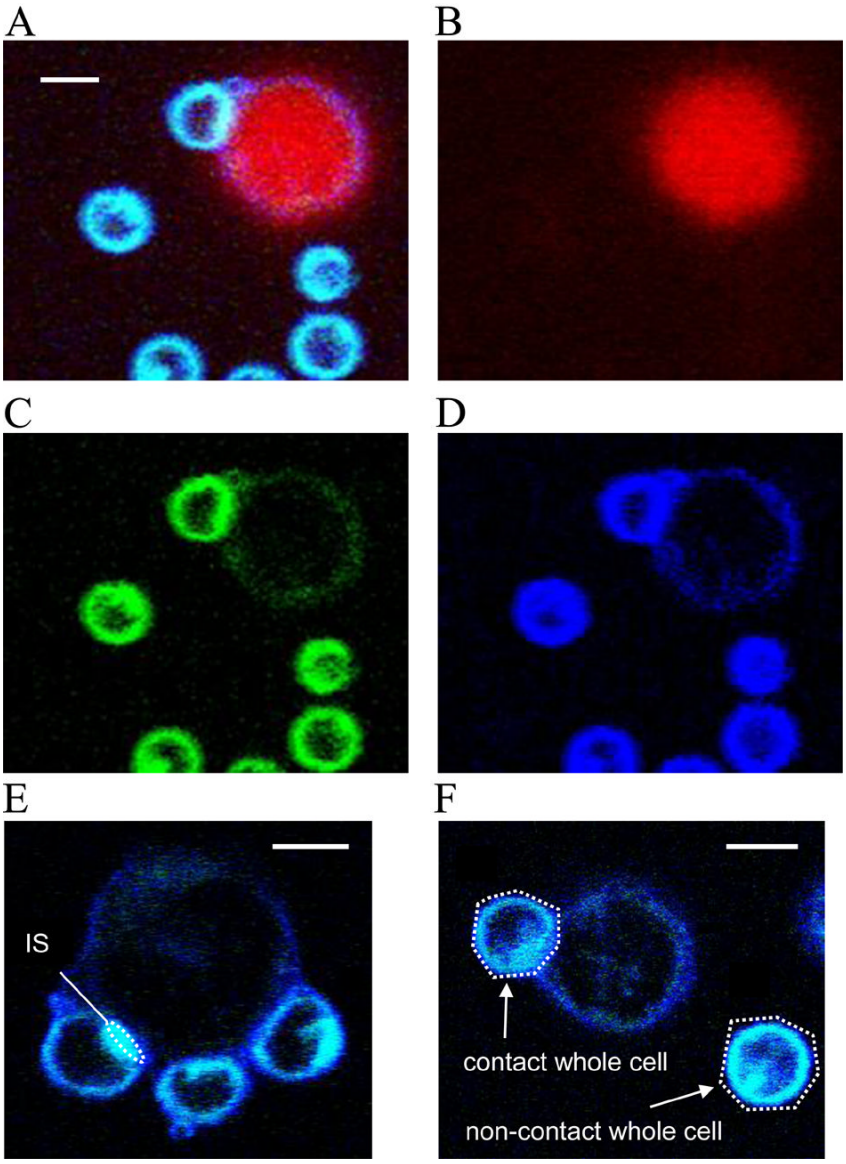

Fig. 1.

Representative two-photon microscopy images of the Laurdan labeled T cells. 8-bit TIFF format captured images were analyzed in (A) RGB, (B) red (CMTMR), (C) green ($I_{470-530}$) or (D) blue ($I_{400-460}$) channels, respectively. Regions of interest (ROI) at (E) T cell immune synapse, (F) contact whole cell and non-contact whole cell were selected by drawing an oval or polygon as shown in white dotted lines. Mean intensities from blue and green channels were recorded to calculate GP-values as described in the Methods. Scale bar, 5 μm.

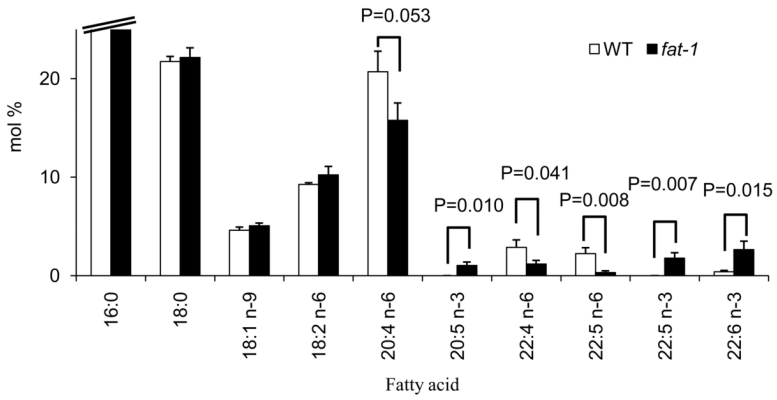

Fig. 2.

Major fatty acid composition of $CD4^+$ T cell total lipids in WT and *fat-1* mice. Splenic $CD4^+$ T cells were isolated from wild type (WT) or *fat-1* transgenic mice. Total phospholipids were isolated and fatty acid composition was analyzed by gas chromatography, n=5.

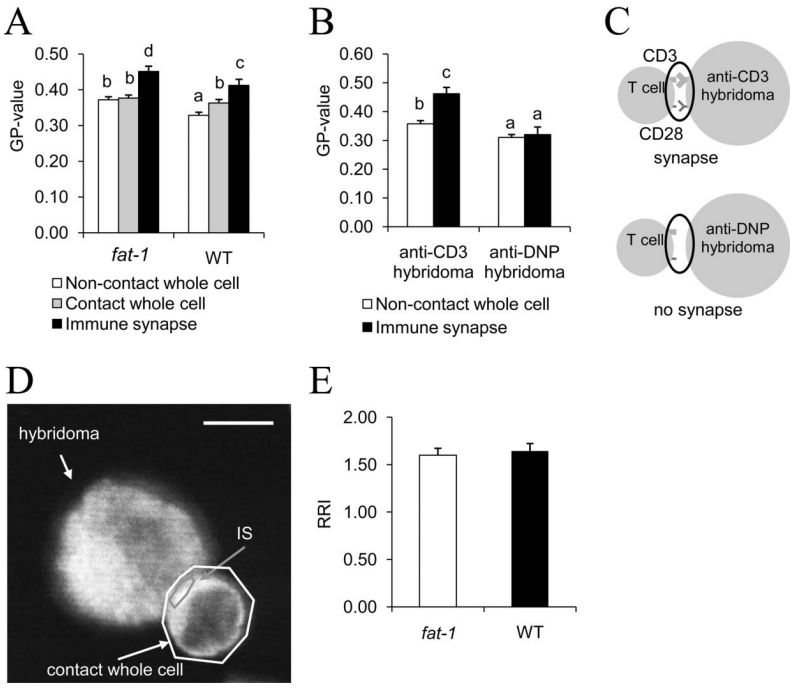

Fig. 3.

Lipid raft formation and GM1 relocalization at the IS of $CD4^+$ T cells. (A) GP-values, which indicate microenvironment fluidity in the plasma membrane, were quantified in $CD4^+$ T cells obtained from either *fat-1* or WT mice (8-14 cells per mouse from 3-4 mice per genotype were examined to obtain a total of n=27-51 observations). Bars with different letters indicate significant differences at $P<0.05$ across all treatment groups within panel A. (B) IS-dependent increase of GP-values was confirmed by anti-DNP hybridoma cells (negative control, n=6-9 cells from one mouse per genotype). Bars with different letters indicate significant differences at $P<0.05$ across all treatment groups within panel B. (C) Schematic of IS formation (top) and non-IS contact (bottom), respectively. (D and E) Immunofluorescence analysis of GM1 recruitment into the IS. Purified $CD4^+$ T cells and anti-CD 3 hybridomas were coincubated, fixed, permeablized, labeled with CTx-FITC. Confocal microscopic images were captured and MFI was measured at the IS relative to the whole cell to calculate RRI, as described in the Methods. (D) Representative image of GM1 localization. Scale bar, 5 μm. (E) The relocation of GM1 at the IS was assessed by RRI of CTx-FITC (n=31-32 cells from 3 mice per genotype).

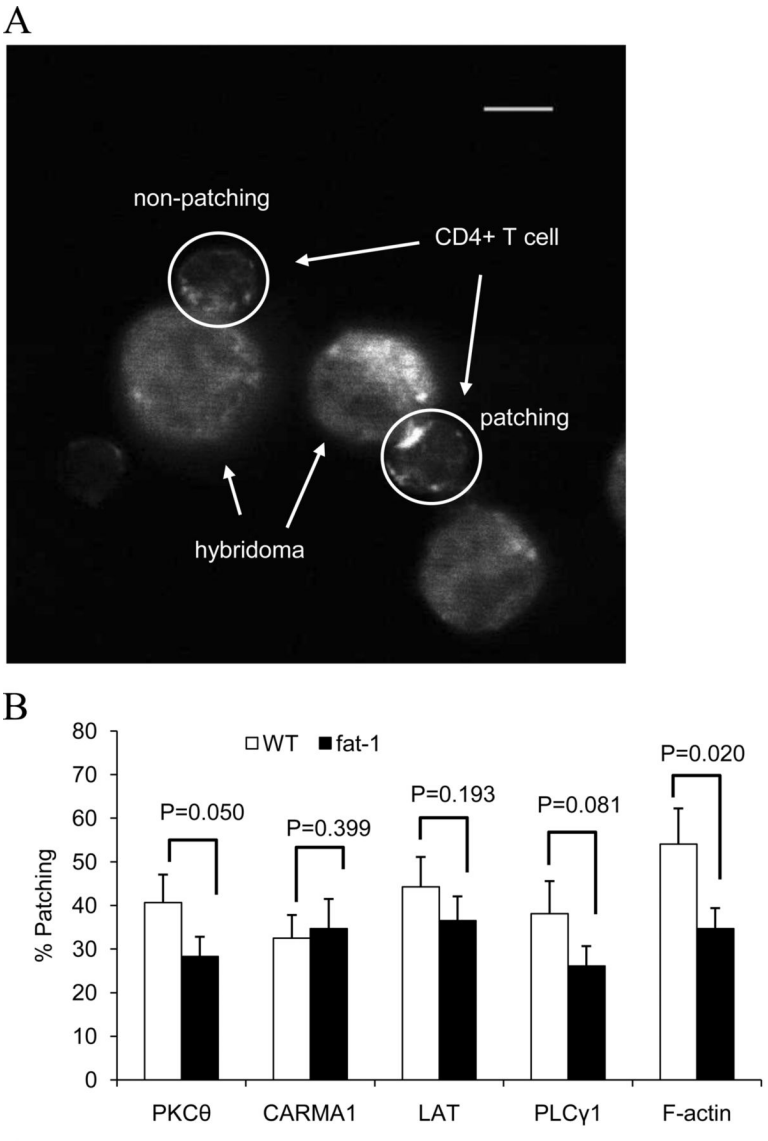

Fig. 4.

Immunofluorescence analysis of localization of signaling molecules into the IS. Purified $CD4^+$ T cells and anti-CD3 hybridomas were coincubated, fixed, permeablized, and labeled with Abs specific to either PKCθ, CARMA1, LAT, PLCγ-1 or F-actin, as described in the Methods. (A) Representative images of LAT localization to the IS in *fat-1* cells. Image contrast was adjusted. Scale bar, 5 μm. (B) Protein localization was assessed by percent patching (the number of patching cells divided by the number of total cells examined, n=37-101 cells from 2-5 mice per genotype for each protein).

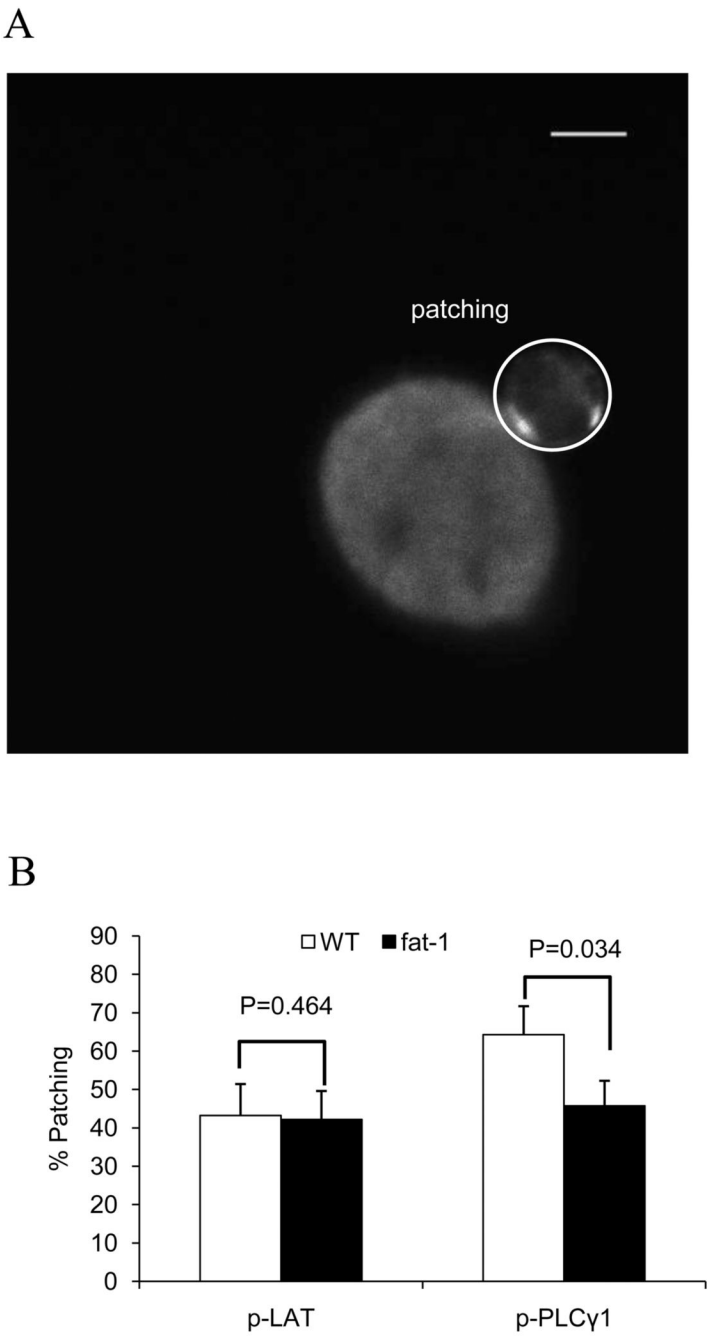

Fig. 5.

Phosphorylation status of signaling proteins at the IS. Purified $CD4^+$ T cells and anti-CD3 hybridomas were coincubated, fixed, permeablized, and labeled with Abs specific to either phospho-LAT or phospho-PLCγ-1, as described in the Methods. (A) Representative image of LAT phosphorylation at the IS in *fat-1* cells. Image contrast was adjusted. Scale bar, 5 μm. (B) Protein activation was assessed by percent patching (n=37-59 cells from 3-4 mice per genotype for each protein).

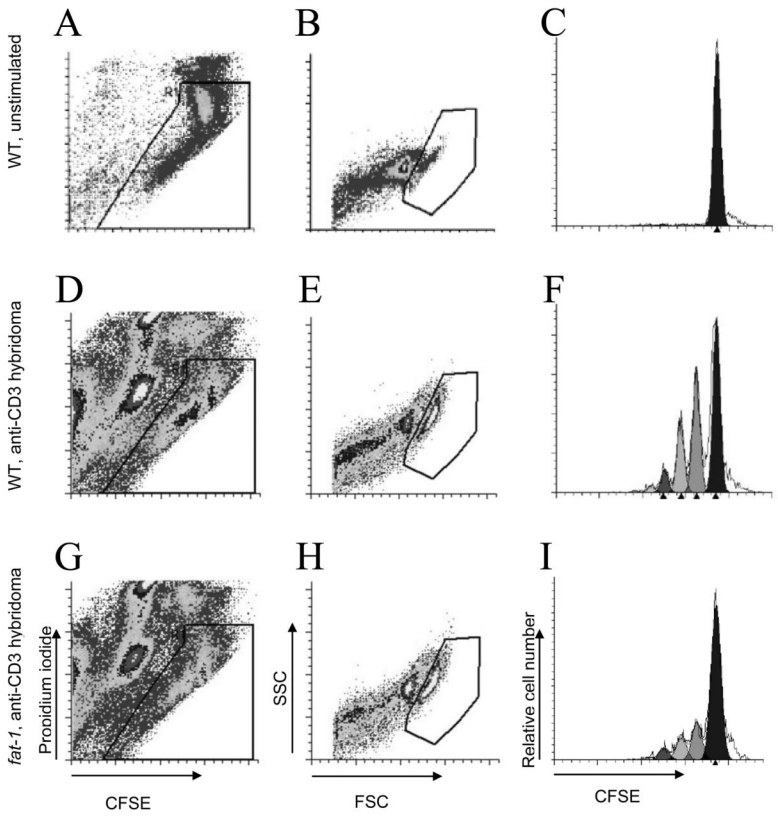

Fig. 6.

Representative CFSE profiles of either basal WT T cells (A-C), anti-CD3 hybridoma stimulated WT (D-F) or *fat-1* (G-I) $CD4^+$ T cells. Regions for viable cells (A, D and G) and lymphocytes (B, E and H) were set based on propidium iodide incorporation and forward/side scatter plots, respectively. Viable lymphocytes were defined as those events falling within both the viability and lymphocyte regions. Computer-aided modeling of each daughter generation (C, F and I) was performed as described in the Methods. The non-divided parental peak was obtained from the unstimulated control group (C). The left shift of peaks (F and G) indicated successive rounds of cell division.

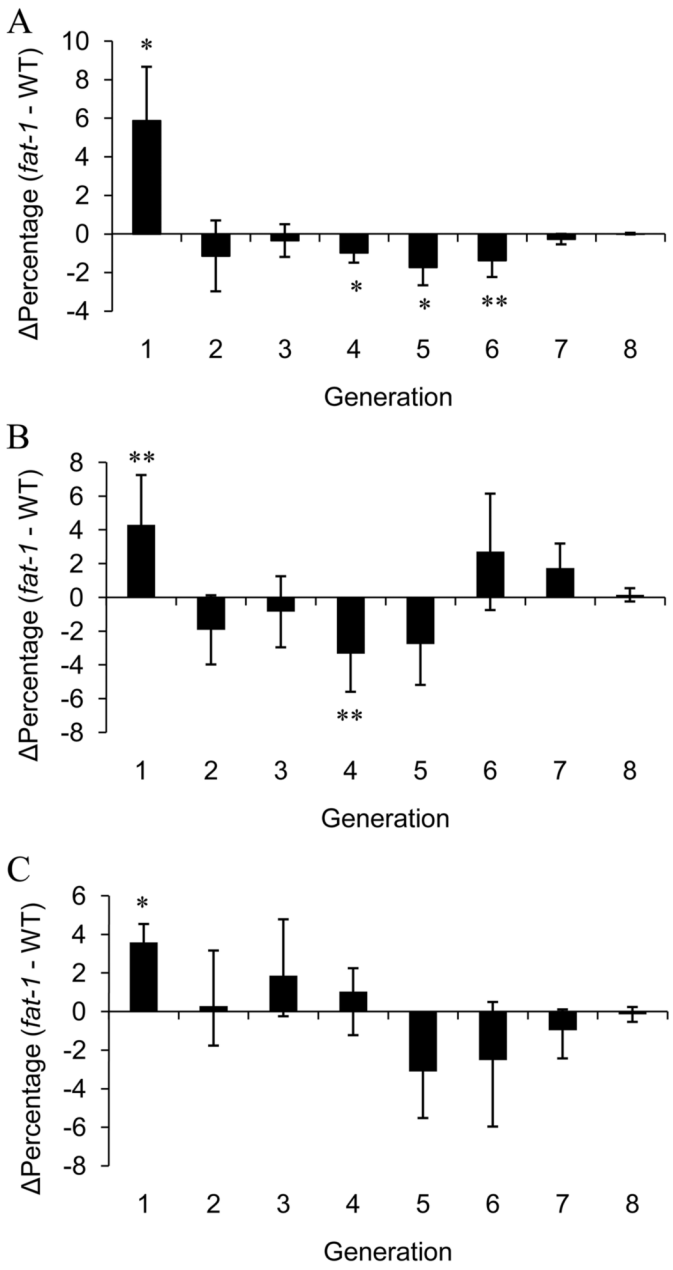

Fig. 7.

The difference in the percentage of T cells (Δpercentage) at each generation was obtained by subtracting the percentage of the WT group from the percentage of *fat-1*. Positive bars show that *fat-1* cultures had more cells in those generations, whereas negative bars show fewer *fat-1* cells. (A) anti-CD3 hybridoma, (B) anti-CD3/28 mAbs and (C) PMA/Ionomycin stimulated (n=6-10 cultures from 3-5 mice per genotype for each stimulus) (*P<0.05, **P<0.10).

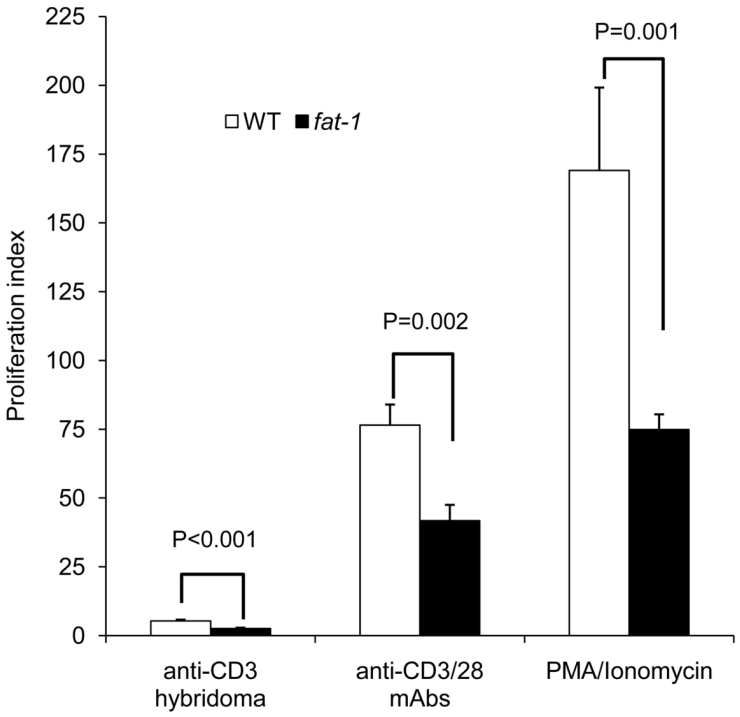

Fig. 8.

The proliferation of $CD4^+$ T cells, expressed as proliferation index (DPM stimulated ÷ DPM unstimulated) in response to either anti-CD3 hybridoma, anti-CD3/28 mAbs or PMA/Ionomycin (n=6-10 cultures from 3-5 mice per genotype for each stimulus).